Available online at www.sciencedirect.com
SCIENCE DIRECT®
Journal of Electron Spectroscopy and Related Phenomena 148 (2005) 80–90
JOURNAL OF ELECTRON SPECTROSCOPY and Related Phenomena
www.elsevier.com/locate/elspec

Alloying of Pd thin films with Nb(0 0 1)

E. Hüger[a,b], H. Wormeester[c], K. Osuch[d,e]*

[a] *Institute of Physics and Physical Technology, Technical University Clausthal, D-38678 Clausthal-Zellerfeld, Germany*
[b] *Department of Biomaterials, IBA e.V. Rosenhof, D-37308 Heilbad Heiligenstadt, Germany*
[c] *MESA+ Research Institute, University of Twente, P.O. Box 217, 7500 AE Enschede, The Netherlands*
[d] *Department of Physics, University of South Africa, P.O. Box 392, Pretoria 0003, South Africa*
[e] *Institute of Mathematics and Physics, University of Podlasie, 3-go Maja 54, 08-110 Siedlce, Poland*

Received 15 June 2004; received in revised form 22 March 2005; accepted 24 March 2005
Available online 10 May 2005

Abstract

Annealing at elevated temperatures (1000–1600 K) of at least 10 ML thick Pd films deposited on Nb(0 0 1) has been found to result in a substrate capped by a pseudomorphic monolayer of Pd. This 1 ML thick Pd cap layer was characterised with a combination of UPS and DFT-calculations. UPS, RHEED and AES show that this cap layer protects the Nb(0 0 1) surface against (oxygen) contamination, which is a well known problem of Nb substrates. AES sputter profiling indicates that a major part of the Pd material in excess of the pseudomorphic monolayer is dissolved in the Nb lattice just below the surface. XPD shows that these dissolved Pd atoms occupy substitutional sites in the substrate. The analysis of the XPS-anisotropy also provides some information about the concentration and positions of the Pd and Nb atoms in the alloyed samples.

PACS: 68.43.-h; 82.80.Pv; 73.20.At; 82.45.Jn; 75.50.Cc; 71.15.Mb

Keywords: Niobium; Palladium; Photoelectron spectroscopy (PES); Surface composition; Electron diffraction

1. Introduction

The bimetallic bonding in binary alloys can lead to new and unique chemical properties of metals. This is a result of significant differences in the band structure of an alloy compared to the band structure of the constituting metals[1]. The largest metal–metal interaction occurs when a binary mixture is made up of an almost fully occupied valence band metal (like Ni and Pd) and an almost empty valence band metal (like Nb and Ta). For novel chemical reactivity properties it is not volume intermixing that is of interest, but rather intermixing in the near surface region and especially at the very surface itself. Many studies of metal–metal bonding have thus focused on Pd deposited on Nb(1 1 0) [1–10] and Ta(1 1 0) [1,10–20]. The adsorption of Pd on Nb or Ta was reported to lead to a reactivity similar to that of Ag [1,15–20]. This dramatic change in chemistry with respect to that observed for the mere Nb and Ta substrate was attributed to a pseudomorphic (ps) monolayer (ML) of Pd adsorbed on Nb(1 1 0) and Ta(1 1 0). However, Nb or Ta substrates fully covered by 1 ps ML of Pd are not easy to obtain because: (i) a phase transition from a commensurate ps Pd structure to an incommensurate Pd(1 1 1) film is observed within the first ML if Pd is deposited by vapour deposition on Nb(1 1 0) or Ta(1 1 0) at or below room temperature[3,12,16] and (ii) the preparation of contamination free Nb and Ta surfaces is not straightforward and contamination hampers the preparation of a substrate capped by a ps ML of Pd. For instance, oxygen contamination is known to negatively change the film growth mechanism and influence the structure of a film[14,15]. (iii) The calibration of exactly 1 ps ML deposited on a substrate is difficult.

A more convenient method of preparing inert, stable, easily reproducible, contamination free Nb or Ta surfaces covered by a ps ML of Pd is to deposit a large quantity of Pd on the substrate surface and subsequently anneal the sample at elevated temperatures [9–13,15,16]. This idea is based on the fact that at high temperatures (1000–1300 K) Pd atoms in excess of 1 ML leave the surface, either through desorption or through diffusion into the substrate. The annealing

* Corresponding author. Tel.: +27 12 4298666; fax: +27 12 4293643.
E-mail address: osuchk@science.unisa.ac.za (K. Osuch).

0368-2048/$ – see front matter © 2005 Elsevier B.V. All rights reserved.
doi:10.1016/j.elspec.2005.03.003

thus leads to Nb(1 1 0) or Ta(1 1 0) substrates covered with 1 ps ML of Pd [9]. Low energy electron diffraction (LEED) indeed shows that this procedure leads to as sharp spots as those obtained from the clean substrate surface [9]. This indicates far better long-range order than that observed for an 'as-deposited' ps Pd. Ultraviolet photoelectron spectroscopy (UPS) measurements show a large similarity between the surfaces obtained with these two methods. The annealing only increases the intensity of the emission features and sharpens them in comparison to those of the 'as-deposited' ps Pd films [10]. Sagurton et al.[9] calibrated the deposition rate of Pd on Nb(1 1 0) through attributing the UPS spectra of an annealed Pd sample to a ps ML of Pd and compared this to the set of UPS spectra collected during the deposition of Pd. Auger electron spectroscopy (AES) measurements of the ps Pd films obtained after annealing showed a higher Pd AES signal than that of the 'as-deposited' ML of Pd [12,15,16]. Koel et al.[16] assigned this to Pd crystallites situated on-top of the ps ML. A comparison of temperature programmed desorption (TPD) data from Pd deposited on Ta(1 1 0) with Pd deposited on W(1 1 0) leads to the conclusion that there also occurs diffusion of Pd into the bulk of Ta. [15,16]. Ruckmann et al. [12] found that the Pd Auger and X-ray photo-electron spectroscopy (XPS) lines show a larger core-level shift for the high temperature annealed substrate. This means that more Pd material with predominantly (nearest neighbour) Pd–Nb bonds must remain after annealing, than in the 'as-deposited' 1 ML Pd sample.

In this paper, we investigate the anneal behaviour of thin Pd films deposited on Nb(0 0 1). X-ray photo-electron diffraction (XPD) and AES sputter-profiling show unambiguously that the annealing procedure leads to the formation of a Pd–Nb alloy just below the surface. Experimental results are further obtained from XPS, reflection high-energy electron diffraction (RHEED) and UPS. The latter measurements are supported by self-consistent density functional theory (DFT) calculations. We show on the grounds of experimental data that the anneal between 1000 and 1500 K of thin Pd films deposited on Nb(0 0 1) leads to: (i) a Nb(0 0 1) surface fully covered by a ps ML of Pd; (ii) the dissolution in a substitutional way of a significant part of the Pd film in excess of the ps ML in the near surface region of the Nb bulk. We first describe the experimental and theoretical methods employed. The presentation and discussion of the data starts by showing that, despite the similar growth of Pd on Nb(0 0 1) and W(0 0 1), the anneal behaviour for Pd deposited on Nb(0 0 1) is very different from that of Pd on W(0 0 1).

2. Experimental setup and electronic structure calculation procedure

2.1. Measurement equipment

The experiments were performed in a VG-ESCA-LAB MKII spectrometer, to which a home-built chamber equipped with a RHEED apparatus was attached. The RHEED chamber was pumped by a titanium sublimation pump with a wall cooled with liquid nitrogen (LN_2) and via the main system by a LN_2-baffled diffusion pump which produces a base pressure of 3×10^{-11} mbar. During the metal deposition from pre-outgassed evaporators situated in both chambers the pressure rose to 7×10^{-11} mbar. The home-built water-cooled metal evaporators allowed deposition rates of 0.03–10 monolayers (ML) per minute.

The surface quality and growth mode were examined with RHEED, AES and angle resolved ultraviolet photoelectron spectroscopy (ARUPS). The geometric structure was determined with RHEED and XPD, the electronic structure with ARUPS. The chemical composition of the sample was checked mainly with AES. A VG-Microtech EX05 ion source was used for sputtering. The ion sputtering was always performed at room temperature. Sputter profiling was done through simultaneous ion sputtering and AES or UPS measurements.

For RHEED measurements, a 20 keV electron beam (emission current 9 μA) at grazing angles of incidence ∼0.3° was used. A Faraday cup detector was used to measure the intensity oscillations of the specular reflected electron beam. The Faraday cup could be moved into any desired position in the central part of the RHEED pattern which was simultaneously observed on a fluorescent screen.

The main chamber (ESCA) contained an hemispherical analyser with the resolution of 60 meV at the pass energy of 2 eV, a monochromatised Al Kα X-ray source and an electron gun for AES, operated at the emission current of 1–3 μA, the beam energy of 1.8 keV, and the beam diameter of 0.2–1 mm at the sample. The Auger signal was differentiated by modulation of the target potential with 3 V (peak-to-peak) for the detection of impurities and with 1 V (peak-to-peak) for in situ monitoring of the film growth. For (AR)UPS measurements a Leybold capillary noble-gas resonance discharge lamp with the photon energy of 21.22 eV (HeI) was used. A polariser made it possible to use both polarised and unpolarised light. For AES and XPS the angular acceptance of the analyser was set to ±12°, for XPD and ARUPS to ±1°.

2.2. Electronic structure calculation

The calculations were performed within the framework of DFT, using the full potential linearised plane wave (FLAPW) method and the local spin density approximation (LSDA) [23,24] as implemented in the Wien2k package [25]. First scalar relativistic calculations were carried out and subsequently spin-orbit coupling was included in a second variation step [25]. A 132 k-points were used in the appropriate irreducible wedge of the Brillouin zone. The adsorption systems were simulated with a slab model, which is known to be very efficient and precise for various surface problems[26]. The unit cell of the slab was for all adsorption systems a tetragon with the height equal to 18 non-relaxed Nb(0 0 1) MLs (18×1.65 Å), and whose base was equal to the two-

dimensional unit cell of the Nb(0 0 1) surface. The unit cell of Pd absorbed on Nb(0 0 1) contained nine Nb(0 0 1) MLs covered by a ps ML of Pd, followed by the free space of 8 MLs. For these systems, the lattice constant in the lateral planes was set to the experimental value of the Nb(0 0 1) substrate (a_{Nb}=3.30 Å), while the vertical positions of the surface and of the first four subsurface layers were optimised through atomic force calculations (z-relaxation) (the derivatives of the total energy with respect to the atomic positions were minimised). Convergence of the self-consistent calculations was assumed when the charge distance defined as $\int |\rho_n(r) - \rho_{n-1}(r)| d^3r$, where ρ is the charge density and n is the iteration number, was smaller then 1×10^{-4}e in three consecutive iterations.

2.3. Preparation of the Nb(0 0 1) surface

The removal of oxygen from Nb and Ta surfaces without serious deterioration of the surface perfection has been a major problem in nearly all the studies of the surfaces in the past [21]. The difficulty of removing oxygen from these surfaces is due to the high solubility and diffusivity of oxygen in these metals and also due to the low vapour pressure of its suboxides. For example in Nb, the solubility has the maximum of 6 atomic percent at about 2050 K and decreases in the absence of an oxygen-containing ambient only above this temperature due to the desorption in the form of NbO and NbO_2. Even in UHV clean Nb absorbs oxygen at partial pressures [22] above 10^{-11} mbar. Thus, there is always an equilibrium concentration of oxygen in bulk Nb which acts as a source of surface oxygen upon the cooling of the heated Nb. We will, therefore, extensively describe the procedure used in the preparation of the substrate surface.

A Nb single crystal (6 mm × 10 mm × 0.5 mm) was mirror-like polished and oriented to within 0.04° of the (0 0 1) face. The stress of the crystal was minimised by supporting it on a pre-outgassed W disk and using Ta sheet springs. Upon the introduction of the crystal in the UHV system, the AES spectrum was dominated by various contaminants, i.e. O, C and weak N and S peaks. The preparation started by first removing the surface contamination with 1 keV Ar ions incident at the polar angle of 40°. This resulted in strong Nb AES signals, but did not completely remove the C- and O-contaminations. Thus it was followed by sputtering at the energy of 2 keV and the polar angle of incidence of 85°. After sputtering for 60 h a Nb surface was obtained with embedded argon and the Nb/C and Nb/O AES amplitude ratios of 60 and 100, respectively. The surface roughness as a result of the sputtering and the embedded Ar was subsequently removed by heating the sample to 1000 K for some minutes. However, RHEED did not show the (1 × 1) periodicity characteristic of a clean Nb(0 0 1) surface. Instead a p(3 × 1)-reconstruction [27] superimposed by long streaks attributed to one-dimensional disorder was observed[28,29].

The AES spectrum from this reconstructed Nb(0 0 1) surface showed the Nb/C AES and Nb/O AES amplitude ratios of 10 and 4, respectively. Next, sputter-annealing cycles were performed for a month, but resulted only in a reduction of the oxygen concentration. This produced the Nb/O AES amplitude ratio larger than 7 upon annealing. Numerous high flashes up to the Nb melting point (∼2700 K) reduced but not diminished the oxygen contamination. Remarkably, the carbon disappeared completely after heating the sample to 1800 K. We want to note, that in the case of one Nb sample, after flashing it near the melting point for more than 5 months, oxygen depletion did occur, but traces of C appeared, as it had also been reported for V(0 0 1)[35].

In order to deposit Pd on a contamination free Nb surface, the slightly oxygen contaminated Nb(0 0 1) surface was very mildly sputtered just before the deposition. This resulted in a slightly rough, but an almost AES clean surface giving still a clear (1 × 1) RHEED image.

3. Results

3.1. Pd on Nb(0 0 1) and W(0 0 1)

3.1.1. Structure

Fig. 1 shows a series of UPS spectra recorded during the deposition of Pd on Nb(0 0 1) at 300 K. In the initial stages of the deposition, there occur marked changes in the electronic structure of Pd. To understand this growth, a comparison was made with the extensively studied growth of Pd on W(0 0 1)[36,38–40], the main difference between W(0 0 1) and Nb(0 0 1) being their different substrate lattice constants of 3.16 and 3.30 Å, respectively. For both epitaxial systems the Pd film showed electron emissions around −2.8, −1.6 and −0.2 eV. Since, the film thickness was calibrated by correlating coverage estimates done with AES [37], UPS and RHEED intensity oscillations for Pd films deposited on W(0 0 1) [38], we could attribute the UPS emissions situated at −2.8 and −1.7 eV to 1 and 2 ps ML of Pd, respectively [36]. The pseudomorphic growth breaks suddenly down at 2.4 ML of Pd on W(0 0 1). A similar breakdown of pseudomorphic growth occurs also on Nb(0 0 1). RHEED shows that after the pseudomorphic range has been reached, Pd grows on both substrates in (1 1 0) oriented films for which the hexagonal densest packed planes lie perpendicularly to the surface [36,38–40].

3.1.2. Quantum size effects

Fig. 1 shows that the UPS spectra of Pd on Nb(0 0 1) and on W(0 0 1) are different when the thickness of the deposited Pd layer is between 2 and 5 ML. For Pd on Nb(0 0 1) a gradual shift of d-band energies with the film thickness can be seen (Fig. 1a) whereas for Pd on W(0 0 1) there seems to exist different phases that consecutively replace each other (Fig. 1b). We further observe that in the case of the latter system the UPS peak at −1.6 eV is replaced by that situated near the Fermi energy, when the film thickness grows. The same UPS peak is also reached in Pd adsorption on Nb(0 0 1),

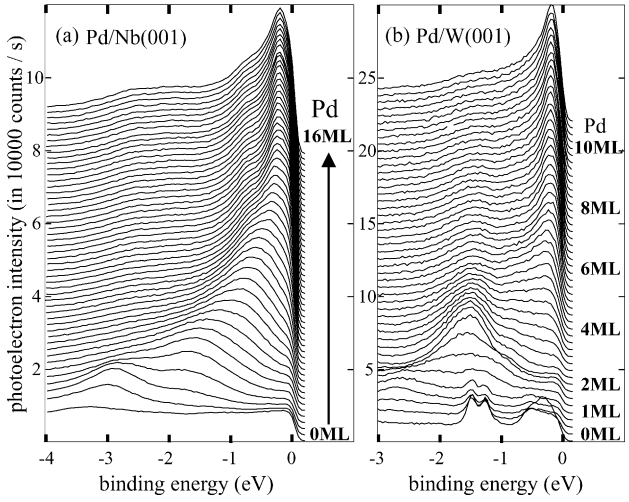

Fig. 1. Normal emission HeI-UPS spectra taken in situ at 300 K during the growth of Pd on (a) Nb(0 0 1) and (b) W(0 0 1).

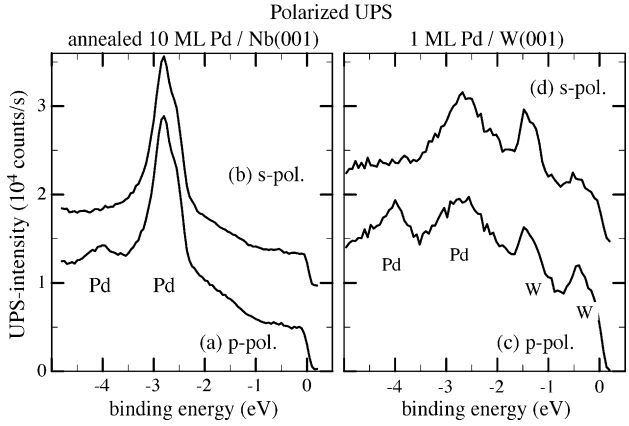

Fig. 2. Normal electron emission HeI-UPS spectra taken with a polarised photon excitation from (a, b) 1 ML of Pd on Nb(0 0 1) and (c, d) 1 ML of Pd on W(0 0 1). Spectra (a, c) were measured with the light polarisation parallel to the plane of incidence (p-polarisation) and spectra (b, d) with the light polarisation perpendicular to the plane of incidence (s('senkrecht')-polarisation). The plane of incidence is the mirror plane lying perpendicularly to the surface which is determined by the incident light and the detected electrons (see for explanation Fig. 6.26 in S. Hüfner [45]).

but, as mentioned above, by a gradual shift. The reason for these differences lies, however, not in different intermediary crystal phases, but rather indifferent intermediary surface morphology, manifesting itself in a different height distribution of the Pd films on Nb(0 0 1) and W(0 0 1) in the thickness range from 2.4 to 5 ML. We observed with RHEED that for Pd deposited on W(0 0 1) at room temperature the Pd material in excess of 2 ML forms 3-dimensional islands with the height of up to 4 MLs. During Pd deposition the islands grow more in lateral directions than in height, continuously reducing the island-free regions of the pseudomorphic, 2 ML thick film. So, on W(0 0 1) UPS should show a continuous replacement of the peak corresponding to the 2 ML thick Pd layer (peak at −1.6 eV) with that characteristic of the 5 (or more) ML thick Pd film (peak near the Fermi energy). Now, in the case of Pd deposited on Nb(0 0 1), RHEED shows a smoother surface, also in the thickness range from 2.4 to 5 ML. The evolution of the UPS spectra of a Pd film on Nb(0 0 1) in the thickness range up to 5 or 6 ML consists in a gradual shift of the binding energy corresponding to the discrete nature of the film thickness, which changes ML by ML. This effect is known as the quantum size effect [41–44]. The wave-lengths (wave-vectors) of the quantum well states (QWS) that occur in the film and their energies (when the quantised band has dispersion) are strongly related to the film thickness. This is so due to the fact that only those quantum well states can exist in the film whose halve-wave-length multiplied by an integer number fits into the film thickness. Confined states (QWS) also exist in Pd films deposited on W(0 0 1), but their energies do not change with the film thickness due to the fact that this change is not discrete (not ML by ML). In the range from 2 to 5 ML, UPS detects in Pd on W(0 0 1) photoelectrons emitted from QWS which correspond only to the thickness of 2, 5 or more MLs. With the growing thickness of the Pd film only the 5 or more ML thick areas increase at the cost of the 2 ML thick ones, and hence the UPS peak near the Fermi energy enlarges, whereas that at −1.6 eV becomes smaller. In contrast, during the growth of Pd on Nb(0 0 1), QWS corresponding to the film thickness of 2-5 ML are gradually formed, which causes the continuous shift of the binding energies observed in UPS. Such a gradual shift is also observed for Pd on W(0 0 1), when Pd films in the range from 2.4 to 5 MLs are smoother. This happens when the deposition of Pd on W(0 0 1) is done at 150 K [38,44].

3.1.3. Polarised UPS

The similarity between the growth of 1 ML of Pd on Nb(0 0 1) and on W(0 0 1) was further investigated with polarised UPS (see Fig. 2), which enabled us to determine the orbital character of the emitted states[45]. The UPS spectra shown in Fig. 2 were recorded at normal electron emission. This implies that the electrons originated predominantly from the states with the orbital character extending in the surface normal direction (the z direction), i.e. the $d_{3z^2-r^2}$ and $d_{xz,yz}$ states, as only these states (beside *s*- and p_z-states) are probed by UPS as a result of the dipole-selection rule [46]. The UPS feature at −4.1 eV was observed in Pd on Nb(0 0 1) only with the polarisation parallel to the plane of incidence of light, which relates it to states with the $d_{3z^2-r^2}$ orbital character. Features that could be observed with the both polarisations, as the feature at −2.8 eV, are related to states with the $d_{xz,yz}$ orbital character [45]. Pd on W(0 0 1) shows similar properties of the Pd related states.

3.2. Anneal behaviour of the Pd film

The similarity in the growth and electronic structure of Pd deposited at low temperatures on Nb(0 0 1) and W(0 0 1)

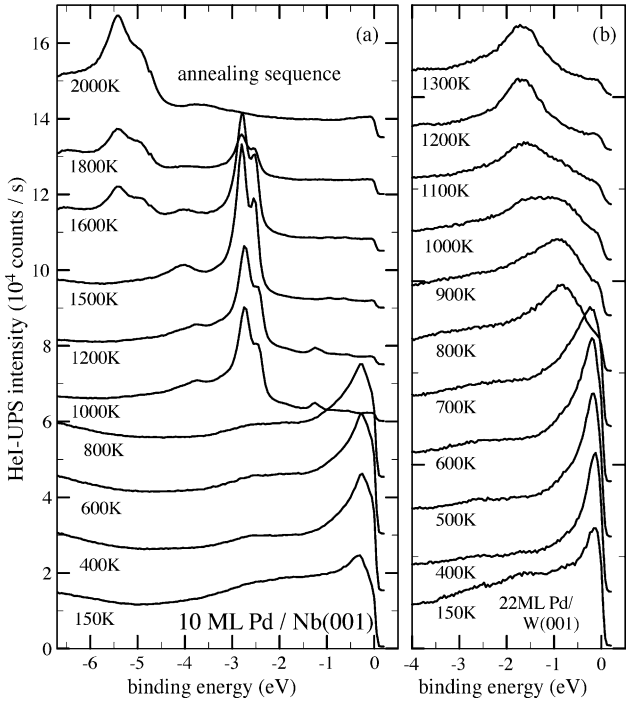

Fig. 3. Normal emission HeI-UPS spectra taken at 150 K after a sequential anneal at the indicated temperatures of (a) a 10 ML thick Pd film deposited at 150 K on Nb(0 0 1) and (b) a 22 ML thick Pd film deposited at 150 K on W(0 0 1). Each anneal lasted 90 s. The features around −5.5 eV above 1500 K are the result of O segregated to the Nb(0 0 1) surface.

should not be extrapolated to the similarity of the film properties upon annealing to temperatures above 800 K. Fig. 3 shows the normal emission UPS spectra recorded after an anneal of a 10 ML Pd film deposited on Nb(0 0 1) at 150 K (Fig. 3a) and a 22 ML Pd film deposited on W(0 0 1) (Fig. 3b). The UPS spectra of Pd on Nb(0 0 1) and W(0 0 1) are similar for up to ∼800 K. Above 800 K, the Pd layer on W(0 0 1) changes due to agglomeration and at 1200 K its UPS spectrum is comparable to the spectrum observed after the deposition of two ps ML of Pd (UPS emission at −1.7 eV). Prigge et al. [47] showed on the grounds of TPD data that desorption of Pd occurs in this system above 1200 K. In contrast to Pd on W(0 0 1), UPS indicates that above 1000 K there remains only 1 ps ML of Pd on Nb(0 0 1) (compare Figs. 3 and 1). Further annealing at a temperature above 1500 K leads to the removal of this ps layer and the appearance of features that can be related to adsorbed oxygen (Fig. 3a). A similar difference in the annealing behaviour of Pd films deposited on two different substrate surfaces was reported by Koel et al. [15]. Their TPD data showed that a Pd film on W(1 1 0) has desorption peaks at much lower temperatures than those of the desorption peaks of Pd deposited on Ta(1 1 0). This shows that Pd atoms are not removed by sublimation from 3D-Pd crystallites, but always from nearest-neighbour Pd-Ta bonds, indicating that Pd intermixes with Ta.

3.3. Electronic structure of 1 ps ML of Pd

The UPS spectrum obtained from 10 MLs of Pd deposited on Nb(0 0 1) and subsequently annealed at 1500 K is similar to that of 1 ps layer. This implies that the sample thus obtained represents a very well ordered, one layer thick metal adsorbate. Such a layer is very suitable for further electronic structure characterisation. This can be done by applying a combination of ARUPS and electronic structure calculations. Fig. 4a shows the polar-angle dependent electron emission recorded along the two high symmetry directions of the surface, i.e. the $[1\,0\,0]_{Nb}$ and $[1\,1\,0]_{Nb}$ azimuths. The $k_\parallel$ values of the initial emission states can be calculated from $k_\parallel = (1/\hbar)\sqrt{2m_e E_{\mathrm{kin}}} \cdot \sin\theta = (1/\hbar)\sqrt{2m_e(h\nu - \Phi - |E_B|)} \cdot \sin\theta$ [45], where θ is the emission angle, E_{kin} the kinetic energy of the emitted photoelectrons, Φ the work function of the film, E_B the binding energy of the initial state and $h\nu$ the energy of the photons used. The obtained $E(k_\parallel)$ dispersion is presented in Fig. 4b. A DFT slab calculation of a ps ML of Pd on Nb(0 0 1) results in the dispersion showed in Fig. 4. In the calculation scheme, the interlayer distances were relaxed for both the ps ML of Pd and the first four MLs of Nb. This resulted in the interlayer distance between the Pd and the first Nb layer by 22.3% smaller then the respective volume Nb(0 0 1) interlayer distance. An expansion of 1.8%, a contraction of 1.2%, an ex-

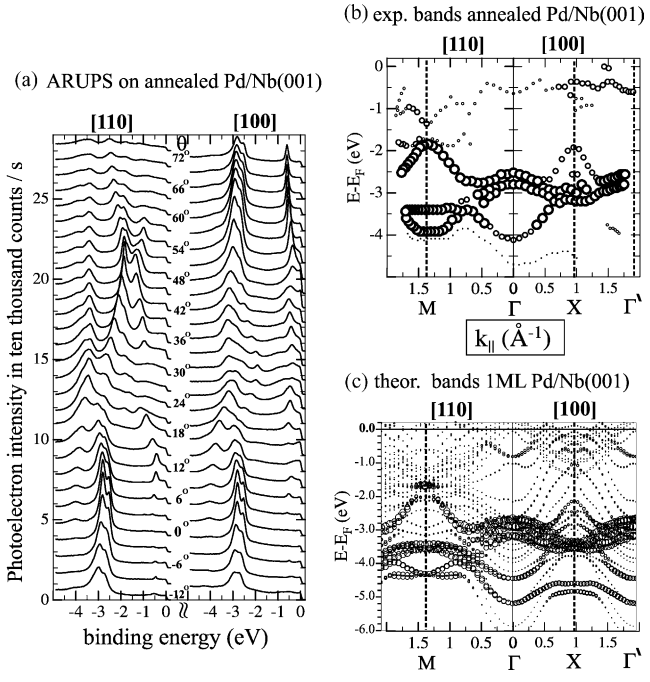

Fig. 4. (a) ARUPS spectra obtained from a 10 ML Pd film deposited on Nb(0 0 1) after the system had been annealed at 1500 K for 90 s. (b) $E(k_\parallel)$ dispersion as obtained from the ARUPS data. Large circles correspond to strong UPS emissions, while smaller circles denote weak electron emission features. (c) $E(k_\parallel)$ dispersion obtained from a DFT calculation of a ps ML of Pd on Nb(0 0 1). The size of the circles is the measure of the local density of states within the Pd layer.

pansion of 1.8%, and a contraction of 4.3% were obtained for the subsequent interlayer distances between the Nb planes. The experimental and theoretical results are quite similar as many of the prominent features present in the calculation are also observed in the experimental dispersion. The features at −2.8 and −4.1 eV are related to the pseudomorphic Pd monolayer absorbed on Nb(0 0 1) [48]. This is further confirmed by RHEED images which show a well ordered ps surface without traces of oxygen.

Both ARUPS and RHEED cannot, however, answer the question whether the layer is completely closed or the Nb(0 0 1) surface is covered by large Pd islands. The presence of 3D crystallites can be ruled out since either their coverage is large and, in this case, the UPS spectrum would show this, or it is small and then transmission features would occur in RHEED. For the comparable system of Co on W(0 0 1) STM showed that no nucleation in the second layer is observed even at coverages close to the completion of the first layer [51]. The large inward relaxation obtained in the calculation of the Pd ML on Nb(0 0 1) indicates the existence of strong Pd–Nb bonds. This points to a large wetting of the Nb(0 0 1) surface by Pd. The nucleation of the second ML is thus also expected to occur only upon completion of the first layer. Therefore, it should be possible to determine whether a sub-monolayer of Pd or a fully covered Nb(0 0 1) substrate is obtained by further depositing Pd on the ps Pd layer obtained after annealing. Fig. 5 shows the UPS spectra taken during this additional deposition of Pd. The UPS features situated at −4.1 and −2.8 eV and assigned to 1 ps ML are clearly attenuated from the start of the deposition, while the feature at −1.6 eV assigned to two ps ML develops immediately (see also Fig. 6). This means that the ps Pd layer obtained after the anneal of a 10 ML Pd film deposited on Nb(0 0 1) to 1500 K completely covers the Nb(0 0 1) substrate.

3.4. Subsurface Pd

Annealed Pd films on Ta [15,16,12] have a Ta surface covered by ps Pd atoms. AES measurements on these samples and also AES measurements performed on the annealed Pd film on Nb(0 0 1) show a Pd signal that corresponds to some 1.3 ML of Pd without traces of contamination (see Fig. 6a). An even larger amount of Pd in the outer layers of the substrate is found with XPS (see Fig. 6b), as a higher kinetic energy (1145 eV) of the Pd-3d electrons in comparison to the Pd AES line (330 eV) results in a larger probing depth. The annealed sample covered with 1 ps Pd ML has a larger intensity of the Pd line as compared to a 2 ML Pd film deposited directly on the Nb(0 0 1) surface. This indicates that, in contrast, to W(0 0 1), annealing the sample at a high temperature does not result in the desorption of Pd, but in its intermixing with the Nb crystal. This was further investigated with AES sputter profiling. The sputter rate was determined by recording the AES signal upon sputtering the Nb(0 0 1) substrate covered with a well known amount of adsorbate. Fig. 7 shows that a ps ML of S bonded to Nb(0 0 1) [39] is sputtered

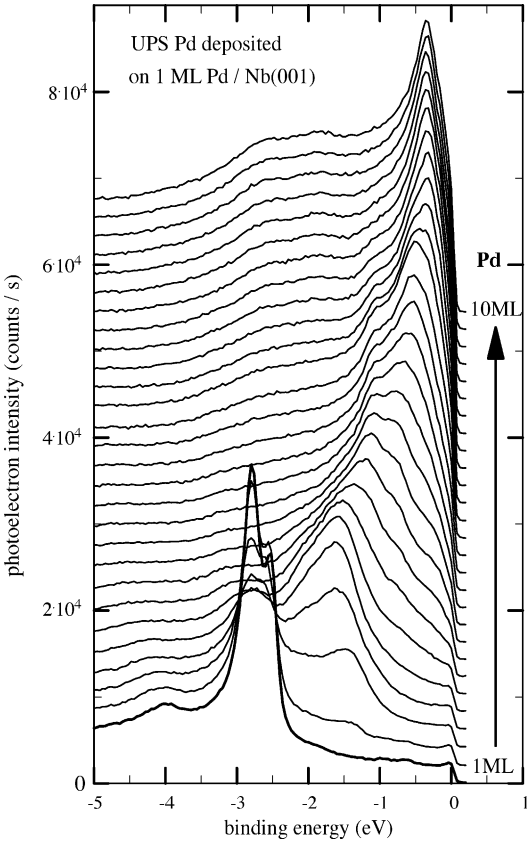

Fig. 5. Normal emission HeI-UPS spectra taken in situ at 150 K during the growth of Pd on an annealed Pd/Nb(0 0 1) sample, as discussed in the text.

away in roughly 8 min. An exponential decay fit to the AES signal strength gives a decay rate of $\tau \simeq 2$ min. A similar experiment was performed for Au and Pd adsorbates. This resulted in the decay rate of $\tau \simeq 2.6$ min. for a 1.2 ML thick film. The both Auger signals of the Pd and Au films with the coverage of 1.2 ML could no longer be detected after 12 min of sputtering. In contrast, the AES Pd signal of the annealed 10 ML film vanished only after some 160 min of sputtering (see Fig. 8). This indicates that the Pd intermixing extends deep into the bulk. The intensity level indicates that

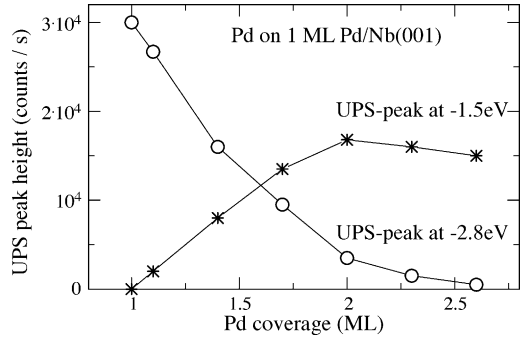

Fig. 6. Background corrected peak heights of the UPS-emissions at −2.8 and −1.5 eV during Pd deposition on the Nb(0 0 1) substrate capped by a ps Pd, see also Fig. 5.

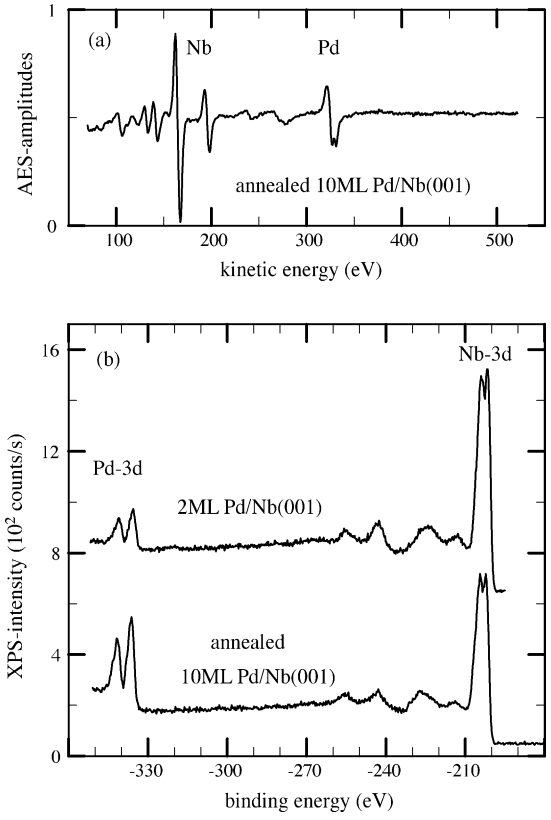

Fig. 7. (a) AES from a 10 ML thick Pd film on Nb(0 0 1) annealed to 1500 K for 90 s. (b) XPS from 2 ML Pd on Nb(0 0 1) deposited at 150 K and an XPS measurement from a 10 ML thick Pd film on Nb(0 0 1) annealed to 1500 K for 90 s. Shown are the Nb-3d and Pd-3d XPS peaks.

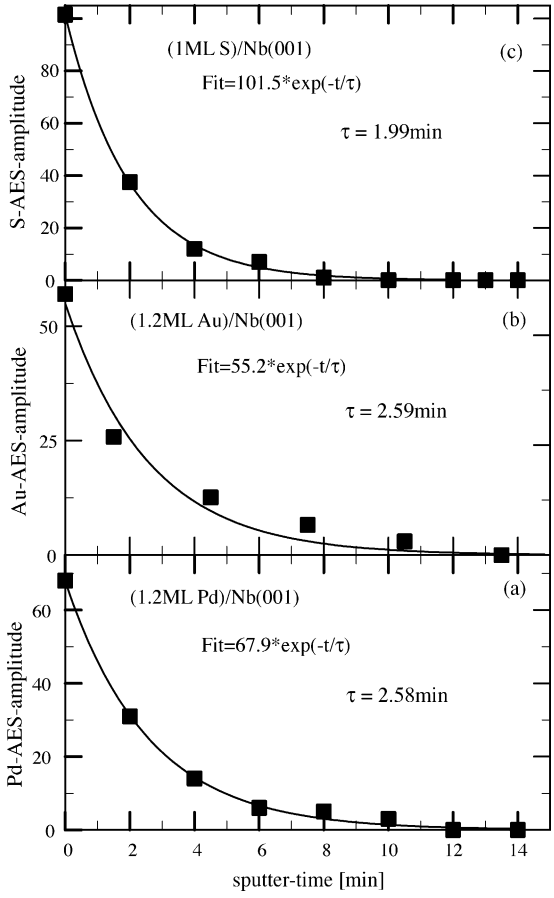

Fig. 8. (a) Auger Pd (330 eV-MVV-line) signal evolution upon Ar sputtering of 1.2 ML 'as-deposited' Pd on Nb(0 0 1). (b) Auger Au (65 eV-NVV-line) signal evolution upon Ar sputtering of 1.2 ML of 'as-deposited' Au on Nb(0 0 1). (c) Auger S (151 eV-line) signal evolution upon Ar sputtering of 1 ML of S on Nb(0 0 1). The continuous lines are the fit of an exponential decay function to the measured points. The sputtering was done with the kinetic energy of the Ar-ions of 1 keV, and at the sputtering-angle of 42° from the surface normal direction.

just below the surface the Pd–Nb layer consist of about 20% of Pd, while the Pd concentration is reduced to 10% after some 100 min. With the decay rate of 2.6 min for 1 ML, the measured subsurface Pd amounts to about 7 ML. This indicates that a large part of the initial 10 ML is left either as the ps cap layer or is found in the subsurface region that is more than 50 layers deep. The rapid decrease of the AES signal of Pd and a similar increase of the Nb signal provides again evidence for the existence of a cap layer.

Next, the role of the thickness of the initially deposited Pd film was investigated. For a 100 ML Pd film, annealing at a slightly higher temperature and for prolonged times also resulted in UPS features characteristic of a ps Pd ML on the Nb(0 0 1) substrate. In this case RHEED did not give any indication of 3D crystallites, either. AES sputter profiling (see Fig. 9) showed that the concentration of Pd in the subsurface region is higher and extends over a much larger number of layers.

XPD[52–54] provides direct information in real space of the 3D crystalline structure of the outer layers of the substrate. This information is accessible for atomically flat films only with diffraction methods in combination with extensive calculations. Forward scattering of electrons, which is at the origin of this technique, increases with the increasing electron kinetic energy and with the decrease of the inter-atomic distances along a specific crystalline direction. Thus, XPD could be used to determine that not only was Pd present in subsurface positions, but also that these positions were substitutional ones.

Figs. 10 and 11 show the emission angle distribution of the XPS Nb-3d emission line scanned along the [1 1 0] (Fig. 10) and [1 0 0] (Fig. 11) azimuth of various Nb(0 0 1) samples. These distributions were obtained after a background correction. This was done by also measuring the angle distribution of inelastic electrons with the kinetic energy of 1280 eV for Nb and 1050 eV for Pd. The structureless background was multiplied by a constant factor and then subtracted from the elastic signal. The curves of a slightly oxygen contaminated and a slightly sputtered surface (a and b) show strong forward focusing for $\theta = 0^\circ$ and 55° along the [1 1 0]-azimuth and for $\theta = 0^\circ$ and 45° in the [1 0 0] azimuth. These angles correspond to the densely-packed crystalline directions in the bcc substrate (see Fig. 12). Similar angular distributions for a Nb(0 0 1) substrate were obtained experimentally and

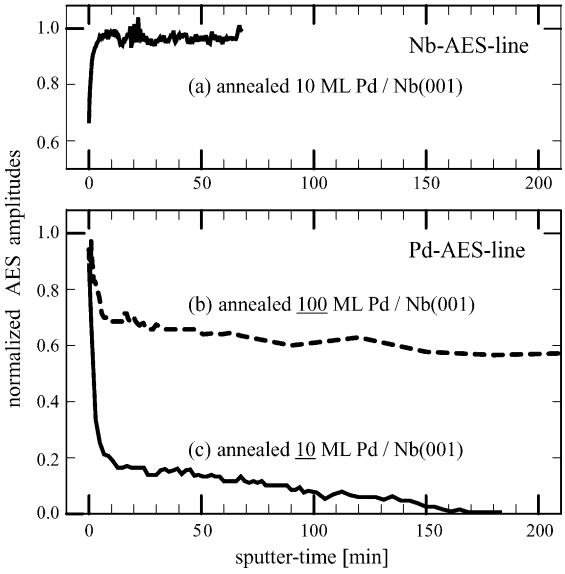

Fig. 9. AES amplitudes of the 167 eV-MVV Nb line (curve marked with (a)) and of the 330 eV MVV Pd line (curve marked with (b) and (c)) during the Ar sputtering of 'annealed Pd' samples. Curves (a, c) refer to he samples obtained by an anneal to 1500 K of a 10 ML thick Pd film deposited on Nb(0 0 1) for 90 s, whereas curve (b) corresponds to the sputtering of a 100 ML thick Pd film after it was annealed for 120 s to 1600 K. The sputtering was done with the kinetic energy of the Ar ions of 1 keV, at the sputter angle of 42° from the surface normal direction.

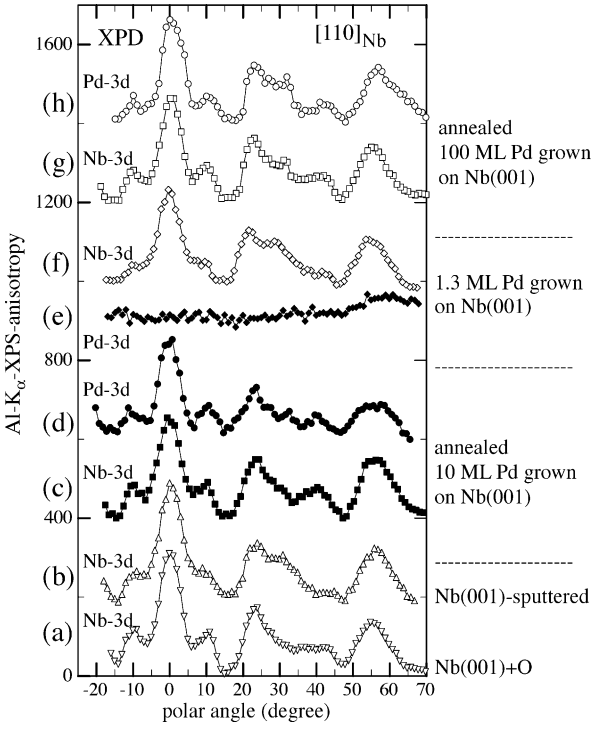

Fig. 10. Polar angle distribution of X-ray photo-electrons along the [1 1 0]-azimuth of the Nb(0 0 1) substrate. The background corrected XPS intensities obtained from: (a) the Nb-3d line of a flat Nb(0 0 1) substrate with a slight amount of oxygen present on the surface; (b) the Nb-3d line of a sputter-cleaned Nb(0 0 1) substrate as used in the deposition experiments; (c) the Nb-3d and (d) the Pd-3d line of a 10 ML film of Pd deposited on Nb(0 0 1) after the film was annealed at 1500 K for 90 s; (e) the Pd-3d and (f) Nb-3d line of a 1.3 ML film of Pd deposited on Nb(0 0 1) at 150 K; (g) the Nb-3d and (h) Pd-3d line of a 100 ML Pd film deposited on Nb(0 0 1) and annealed at 1600 K for 120 s. The surface normal direction corresponds to $\theta = 0^\circ$. The kinetic energy of the Nb-3d (Pd-3d) photoelectrons excited by Al Kα radiation was ~1280 eV (1145 eV). The Pd anisotropies (d, e) and (h) were multiplied by 4 and 1.5, respectively.

theoretically in fully dynamic multiple-scattering calculation of the Nb-3d lines[55]. The dynamic calculations showed that intensity maxima appear along close-packed crystalline axes. The other features were assigned to multiple scattering effects. A layer resolved analysis of these calculations showed that the strong normal emission ($\theta = 0^\circ$) and the feature observed at $\theta = 8^\circ$ are due to electrons scattered by seven to ten monolayers of Nb. In our XPD measurements, these side peaks were observed at the slightly larger polar angle of $\theta = 10^\circ$. This is probably due to a slightly larger kinetic energy of our photo-electrons as we used an Al Kα source instead of the Mg Kα source of Lo et al.[55]

The angular distributions of photo-electrons of both the Pd-3d line (Figs. 10d,h and 11d,f) and the Nb-3d-line (Figs. 10a,b,c,f,g and 11a,b,c,e) of the annealed Pd film are similar. These angular distributions are also similar to those measured and calculated by Lo et al. [55] A 1.3 ML film of Pd (Fig. 10e) does not show any features[56], confirming that the intermixing takes place after annealing at elevated temperatures. The similarity between the Nb and Pd lines clearly shows that a large concentration of Pd atoms exists in the subsurface and that these Pd atoms are in substitutional positions. The modulation observed also indicates that this subsurface layer containing Pd is at least 7–10 layers deep.

An even more important piece of information which can be extracted from the XPD data is the strength of the diffraction effect. Fig. 13 shows the anisotropy of the overall XPS intensity for the main XPD peaks, calculated as $[(I_{max} - I_{min})/I_{max}]\%$, where I_{max} is the overall XPS signal and $I_{max} - I_{min}$ is the XPD peak height. These true anisotropy values contain important information about the depth distribution of the atoms (e.g. Pd atoms). The contribution of the surface ML to the measured XPS intensity is large (top layer), but its contribution to the measured anisotropy is essentially zero (no forward scattering). This means that if the annealed Pd/Nb samples are capped by Pd, the diffraction effect (anisotropy) in the Nb signal should be much more stronger than in the Pd signal, because the Pd signal originates mostly from the surface ML whose contribution to the anisotropy of the Pd signal is negligible. Exactly this is observed in Fig. 13. Firstly, the Nb signal obtained from the annealed Pd/Nb samples shows an higher anisotropy than that of the clean Nb(0 0 1) sample and, secondly, it is much larger than the Pd signal. This means that Nb signal from the annealed Pd/Nb samples has no featureless intensity contribution from the top layer, which in turn, implies that the annealed Pd/Nb samples are capped by Pd. This is also the reason for the lower anisotropy values of the Pd-XPS sig-

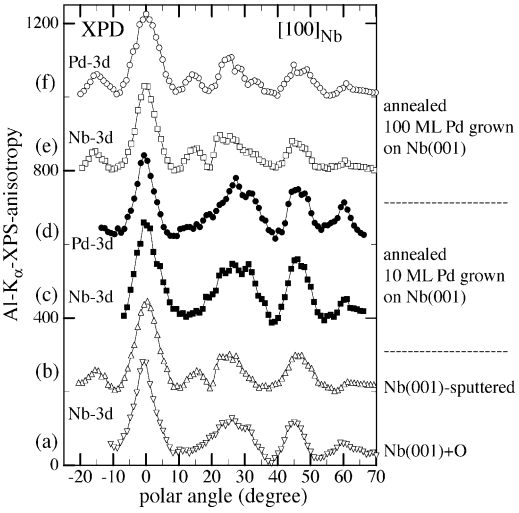

Fig. 11. Polar angle distribution of X-ray photo-electrons along the [1 0 0]-azimuth of the Nb(0 0 1) substrate. The background corrected XPS intensities were measured from: (a) the Nb-3d line of a flat Nb(0 0 1) substrate with a slight amount of oxygen present on the surface; (b) the Nb-3d line of the sputter-cleaned Nb(0 0 1) substrate as used in the deposition experiments; (c) the Nb-3d and (d) Pd-3d line of a 10 ML film of Pd deposited on Nb(0 0 1) after the film was annealed at 1500 K for 90 s; (e) the Nb-3d and (f) Pd-3d line of a 100 ML Pd film deposited on Nb(0 0 1) and annealed at 1600 K for 120 s. The surface normal direction corresponds to $\theta = 0^\circ$. The Pd anisotropies (d) and (f)) were multiplied by 4 and 1.5, respectively.

nal. The Pd anisotropy of the annealed 10 MLs of Pd on Nb(0 0 1) is the smallest, because the capping Pd layer contributes strongly to the overall Pd-XPS signal, without contributing to its anisotropy. The Pd-XPS anisotropy of the annealed 100 MLs of Pd on Nb(0 0 1) is larger than that of the

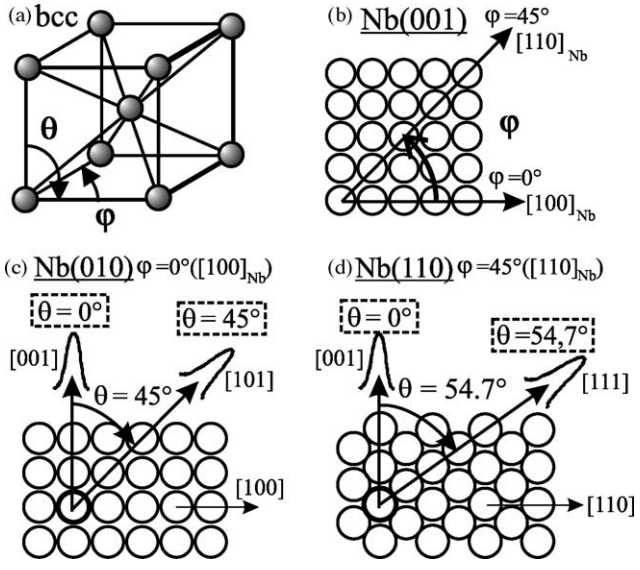

Fig. 12. (a) Sketch of the body-centred cubic lattice depicting the emission angles. Azimuthal angle (ϕ) was changed in the surface plane of Nb(0 0 1) (panel (a, b)). Polar angle (θ) was measured in the plane perpendicular to the surface, and along the high symmetry azimuth directions [1 0 0] (c) and [1 1 0] (d).

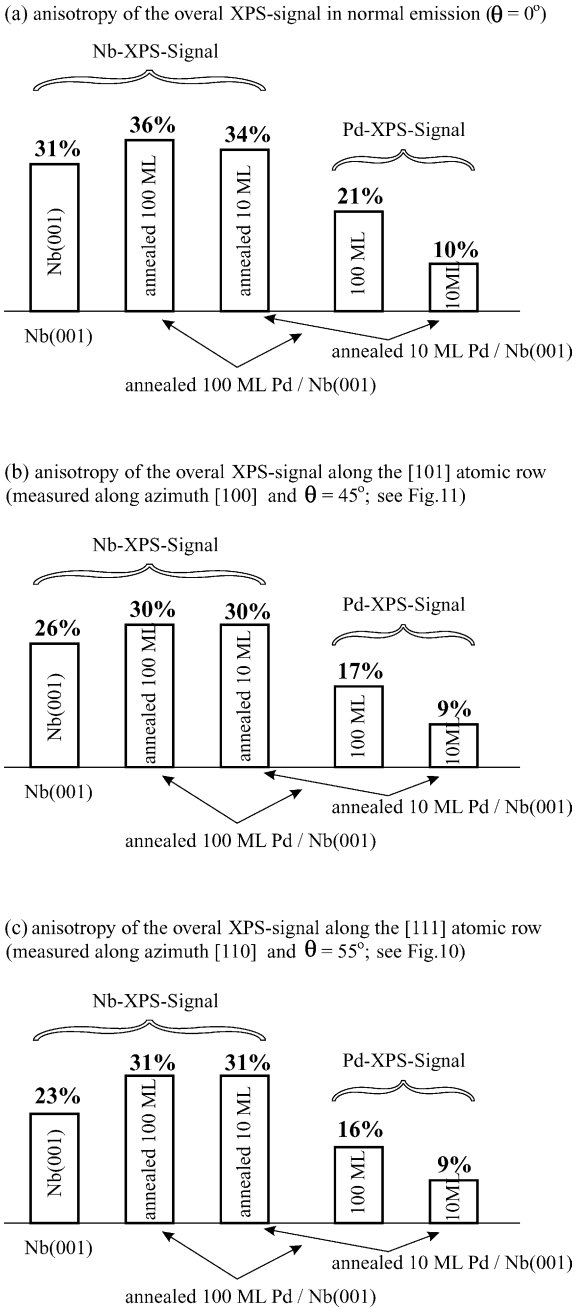

Fig. 13. Strength of the diffraction effect in comparison to the overall XPS signal, for forward-focusing along the main crystallographic axis (see Fig. 12), calculated as $[(I_{max} - I_{min})/I_{max}] \cdot \%$, where I_{max} is the overall XPS signal and $I_{max} - I_{min}$ is the XPD-peak height. (a) True anisotropy of the normal emission peak ($\theta = 0^\circ$) which occurs due to the forward-focusing along the [0 0 1] atomic row (see Fig. 12c,d). (b) True anisotropy of the diffraction at the [101] atomic row. The forward-focusing peak was measured in the [1 0 0]-azimuth at $\theta = 45^\circ$ (Fig. 11). (b) True anisotropy of the diffraction at the [1 1 1] atomic row. The signal was measured in the [1 1 0] azimuth at ($\theta = 55^\circ$) (Fig. 10). Represented in each panel are the anisotropies of the Nb-3d and Pd-3d XPS signals of a clean and lightly sputter-rough Nb(0 0 1) substrate, 100 ML Pd/Nb(0 0 1) annealed at 1600 K and of 10 ML Pd/Nb(0 0 1) annealed at 1500 K.

annealed 10 MLs of Pd on Nb(0 0 1). This proves that the Pd concentration in the Pd–Nb alloy is higher for the annealed 100 MLs of Pd on Nb(0 0 1), in agreement with the AES-sputter profiles. The overall Pd intensity of the annealed 100 MLs of Pd on Nb(0 0 1) is increased due to the contribution from the XPS intensity of the subsurface Pd atoms which have a higher concentration than in the case of the annealed 10 ML Pd film.

More information about the upper limit of the Pd concentration in the bulk alloy can be inferred from the crystal structure as determined with XPD. The XPD curves of Figs. 10g,h and 11e,f obtained from the annealed 100 ML Pd film show that the formed Pd–Nb alloy has the (0 0 1)-oriented bcc structure without tetragonal deformations. It means that the Pd concentration does not exceed the minimum concentration which induces deformation of the bcc structure. According to the published data on binary alloys [57], Nb–Pd bulk alloys with the concentration of less than 33% (i.e. Nb_2Pd_1) maintain the bcc crystal phase. Thus, the XPD data provides some evidence that the upper limit of the Pd concentration in the formed Pd–Nb subsurface alloy does not exceed 33%. It should be emphasised, however, that these arguments based on bulk phase diagrams are very crude, because the occurrence of new phase boundaries in films up to 10 ML thick is nothing unusual, with this thickness being the upper limit of XPD measurements.

4. Summary

The combination of RHEED-, AES-, XPS-, ARUPS-, AES-sputter profile, XPD-measurements and DFT-calculations for Pd films (10–100 ML) grown on Nb(0 0 1) show that annealing between 1000 and 1600 K leads to a Nb(0 0 1) surface capped with a ps ML of Pd. A major part of the Pd atoms in excess of the ps ML dissolves upon annealing in the Nb substrate in a substitutional way. The diffused Pd intermixes with Nb in the subsurface region forming a Pd–Nb alloy with a bcc-like structure. Sputter-profile measurements indicate that the alloyed region has a quite homogeneous composition starting from just below the first layer down to at least 50 layers below the surface. The chemical nature of the ps Pd monolayer is very different as compared to a Nb or Pd crystal surface. The reason for this difference is a large change in the electron distribution due to the strong Pd–Nb metal bond. We argue that the formation of a well-defined ps capping monolayer of Pd on Nb(0 0 1) that forms spontaneously upon annealing thick Pd films on this substrate, with surplus quantities of Pd dissolved substitutionally in the Nb-lattice, is not restricted exclusively to the Pd/Nb(0 0 1) system. It should also occur for Ta, Nb and V substrates independently from their (0 0 1) or (0 1 1) orientation. Also in those cases, the chemical nature of the ps ML of Pd and of the Pd atoms dissolved in the bulk of Ta, Nb or V should be different as compared to the surface or bulk of Ta, Nb, V, or Pd.

References

[1] J.A. Rodriguez, D.W. Goodman, Science 257 (1992) 897;
J.A. Rodriguez, D.W. Goodman, J. Phys. Chem. 95 (1991) 4196;
J.A. Rodriguez, Surf. Sci. Rep. 24 (1996) 223 and references therein.
[2] M.A. Pick, J.W. Davenport, M. Strongin, G.J. Dienes, Phys. Rev. Lett. 43 (1979) 286.
[3] M. Strongin, M. El-Batanouny, M.A. Pick, Phys. Rev. B 22 (1980) 3126.
[4] M. El-Batanouny, M. Strongin, G.P. Williams, J. Colbert, Phys. Rev. Lett. 46 (1981) 269.
[5] G.P. Williams, M. El-Batanouny, J. Colbert, E. Jensen, T.N. Rhodin, Phys. Rev. B 25 (1982) 3658.
[6] M. El-Batanouny, D.R. Hamann, S.R. Shubb, J.W. Davenport, Phys. Rev. B 27 (1983) 2575.
[7] J.P. Muscat, Surf. Sci. 131 (1983) 299.
[8] V. Kumar, K.H. Bennemann, Phys. Rev. B 28 (1983) 3138.
[9] M. Sagurton, M. Strongin, F. Jona, J. Colbert, Phys. Rev. B 28 (1983) 4075.
[10] M.W. Ruckman, M. Strongin, Phys. Rev. B 29 (1984) 7105.
[11] M.W. Ruckman, P.D. Johnson, M. Strongin, Phys. Rev. B 31 (1985) 3405.
[12] M.W. Ruckman, V. Murgai, M. Strongin, Phys. Rev. B 34 (1986) 6759.
[13] M.W. Ruckman, M. Strongin, Phys. Rev. B 35 (1987) 487.
[14] M.W. Ruckman, L.Q. Jiang, M. Strongin, Surf. Sci. 221 (1989) 144.
[15] B.E. Koel, R.J. Smith, P.J. Berlowitz, Surf. Sci. 231 (1990) 325.
[16] A. Sellidj, B.E. Koel, Surf. Sci. 281 (1993) 223.
[17] A. Sellidj, B.E. Koel, Surf. Sci. 284 (1993) 139.
[18] J.M. Heitzinger, A. Avoyan, B.E. Koel, Surf. Sci. 294 (1993) 251.
[19] D.E. Beck, J.M. Heitzinger, A. Avoyan, B.E. Koel, Surf. Sci. 491 (2001) 48.
[20] J.M. Heitzinger, D.E. Beck, B.E. Koel, Surf. Sci. 491 (2001) 63.
[21] E. Bauer, private communication.
[22] L. Gmelin, R.J. Meyer, E.H.E. Pietsch, E. Fluck, Gmelin's Handbook of Inorganic and Organometallic Chemistry, vol. 49 B1, Verlag Chemie, Berlin, 1925.
[23] P. Hohenberg, W. Kohn, Phys. Rev. 136 (1964) B864.
[24] W. Kohn, L.J. Sham, Phys. Rev. 140 (1964) A1133.
[25] P. Blaha, K. Schwarz, G.K.H. Madsen, D. Kvasnicka, J. Luitz, WIEN2k, An Augmented Plane Wave + Local Orbitals Program for Calculating Crystal Properties, Karlheinz Schwarz, Techn. Universität Wien, Austria, 2001, 3-9501031-1-2.
[26] R. Wu, A.J. Freeman, Phys. Rev. B 52 (1995) 12419.
[27] E. Hulpke, M. Hüppauff, D.-M. Smilgies, A.D. Kulkarni, F.W. de Wette, Phys. Rev. B 45 (1992) 1820;
P. Turban, L. Hennet, S. Andrieu, Surf. Sci. 446 (2000) 241;
H.H. Farrell, M. Strongin, Surf. Sci. 38 (1973) 18.
[28] B. An, S. Fukuyama, K. Yokogawa, M. Yoshimura, Phys. Rev. B 68 (2003) 115423.
[29] There is a collection of experimental results, which shows that oxygen commonly induces periodic atomic corrugations on thesurface of noble and transition metals [30,31], including Ta(0 0 1)-[32,33] and Nb(1 1 0)-surfaces [34], in the form of one-dimensional gratings.
[30] T. Schröder, I.B. Giorgi, A. Hammoudeh, N. Magg, M. Bäumer, H.-J. Freund, Phys. Rev. B 65 (2002) 115411 and references therein.
[31] F. Besenbacher, I. Stensgaard, D.A. King, D.P. Woodruff (Eds.), The Chemical Physics of Solid Surfaces and Heterogeneous Catalysis, vol. 7, Elsevier, Amsterdam, 1994, p. 573;
F. Besenbacher, J.K. Nø rskov, Prog. Surf. Sci. 44 (1993) 5 and references therein.
[32] B.J. Hopkins, M. Leggett, G.D. Watts, Surf. Sci. 28 (1971) 581.
[33] A.V. Titov, H. Jagodzinski, Surf. Sci. 152/153 (1985) 409.
[34] Ch. Sürgers, M. Schöck, H.v. Löhneysen, Surf. Sci. 471 (2001) 209.
[35] R. Koller, W. Bergermayer, G. Kresse, E.L.D. Hebenstreit, C. Konvicka, M. Schmid, R. Poudloucky, P. Varga, Surf. Sci. 480 (2001) 11.
[36] H. Wormeester, E. Hüger, E. Bauer, Phys. Rev. Lett. 77 (1996) 1540.

[37] E. Hüger, K. Osuch, Europhys. Lett. 62 (2003) 278.
[38] H. Wormeester, E. Hüger, E. Bauer, Phys. Rev. B 54 (1996) 17108.
[39] H. Wormeester, E. Hüger, E. Bauer, Phys. Rev. Lett. 81 (1998) 854.
[40] E. Hueger, H. Wormeester, E. Bauer, Surf. Sci. 438 (1999) 185.
[41] E. Hüger, K. Osuch, Phys. Rev. B 68 (2003) 205424.
[42] E. Hüger, K. Osuch, Eur. Phys. J. B 37 (2004) 149.
[43] E. Hüger, K. Osuch, J. Electron. Spectrosc. Rel. Phenom. 141 (2004) 13.
[44] E. Hüger, K. Osuch, Solid State Commun. 132 (2004) 97.
[45] S. Hüfner, Photoelectron Spectroscopy, Springer, Berlin, 1995.
[46] H. Knoppe, Thesis, TU-Clausthal, 1995.
[47] S. Prigge, H. Roux, E. Bauer, Surf. Sci. 107 (1981) 101.
[48] There are two reasons why peaks observed in UPS come only from Pd bonded to Nb(0 0 1) and not from Nb in deeper layers: (i) the UPS-intensity: for HeI-excitation (21.22 eV), Pd has a three times larger photo-ionisation cross section than Nb [49], and (ii) the escape depth: the HeI-excited photoelectrons from the valence states have in Nb(0 0 1) the escape depth of less than 3 MLs [50].
[49] M. El-Batanouny, M. Strongin, G.P. Williams, Phys. Rev. B 27 (1983) 4580 and references therein.
[50] F.J. Himpsel, J.E. Ortega, G.J. Mankey, R.F. Willis, Adv. Phys. 47 (1998) 511 and references therein.
[51] W. Wulfhekel, T. Gutjahr-Löser, F. Zavaliche, D. Sander, J. Kirschner, Phys. Rev. B 64 (2001) 144422.
[52] S.A. Chambers, Adv. Phys. 40 (1991) 357.
[53] D.P. Woodruff, A.M. Bradshaw, Rep. Prog. Phys. 57 (1994) 1029; D.P. Woodruff, Surf. Sci. 299/300 (1994) 183.
[54] W.F. Egelhoff Jr., J.A.C. Bland, B. Heinrich (Eds.), Ultrathin Magnetic Structures I, Springer, Berlin, 1994, 3-540-57407-7.
[55] W.-S. Lo, T.-S. Chien, B.-S. Fang, C.M. Wei, W.N. Mei, Surf. Rev. Lett. 5 (1998) 1035.
[56] An exception would be the broad signal enhancement around $\theta = 57^{\circ}$ which is caused by forward scattering on the atoms situated in the second ML of the 1.3 ML coverage.
[57] H. Okamoto, T.B. Massalski, Binary Alloy Phase Diagrams, 1985 and references therein.